ChemComm

COMMUNICATION

View Article Online
View Journal | View Issue

Cite this: *Chem. Commun.*, 2024, **60**, 10140

Received 1st July 2024,
Accepted 9th August 2024

DOI: 10.1039/d4cc03267e

rsc.li/chemcomm

Privileged zeolitic sites for humid CO_2 adsorption: K^+ in double eight-membered rings†

Hwangho Lee,*[a] Shu Hikima,[b] Ryohji Ohnishi,[b] Takahiko Takewaki[b] and Alexander Katz*[a]

Humid CO_2 adsorption in K^+-exchanged zeolites featuring double-eight membered ring (D8R) structures results in CO_2 outcompeting and desorbing dimeric water under equilibrated conditions, which is not observed for either the H^+-form of the same zeolites or larger-pore zeolites.

In an effort to combat global warming, there has been a strong focus on capturing CO_2 from post-combustion sources such as flue gas.[1,2] Zeolites, microporous crystalline aluminosilicates, have been extensively investigated in this regard.[3–7] However, an ongoing challenge is the typical observed decrease in CO_2 adsorption capacity due to competitive adsorption by H_2O,[5,8] which generally has a significantly higher heat of adsorption than CO_2.[8,9] Approaches for solving this challenge benefit from selective adsorption sites that preferentially bind quadrupolar CO_2 over dipolar water.[10] Previously, in elegant research that identified key supramolecular interactions involving small-pore zeolite host and CO_2 guest, Lobo *et al.* demonstrated that (i) framework O in eight-membered rings bonds to C atoms of CO_2 by pushing electron density through its lone pairs, and (ii) exchange cations bond to the O atom of CO_2 by pulling electron density and generating an induced dipole in the latter.[11] We posit that cations filling double eight-membered ring (D8R) secondary building units in zeolites have the prospect of fulfilling both (i) and (ii) above, and in doing so, could provide a selective environment for bonding of CO_2 over water, though the structural details of such an environment are currently unavailable. In particular, we demonstrated sites in K^+-exchanged MER zeolite (K-MER) that desorb a water dimer for each CO_2 adsorbed under humid conditions corresponding to 5% relative humidity (RH), with a combined thermogravimetric analysis (TGA) and diffuse reflectance Fourier transform infrared spectroscopy (DRIFTS) approach.[12] These sites were inferred to consist of K^+ cations in D8Rs of K-MER zeolite, which can accommodate either one water dimer or one CO_2 molecule within their volume. Here, we investigate the generality of this last result by studying humid CO_2 adsorption in three new types of zeolites: (i) RHO (Si/Al = 3.7), (ii) MER (Si/Al = 2.9), and (iii) PAU (Si/Al = 3.6) (see Fig. S1, ESI†). These three frameworks were chosen because they contain D8R structures and represent slightly different variations on the symmetry of those structures.[13] TGA data in Fig. 1 show gravimetric profiles upon equilibrated H_2O and humid CO_2 adsorption (5% RH, 1 bar of CO_2 for step II, 30 °C) in these three K^+ ion-exchanged zeolites (Table S1, ESI†). Separate H_2O (in step I) and CO_2 (in step II) uptake in the zeolites was initially evaluated on the basis of the observed weight increases ("TGA only" in Fig. S2, ESI†). These calculated gravimetric uptakes reflect an implicit assumption that CO_2 does not desorb pre-equilibrated H_2O, which will be investigated below (*vide infra*). Interestingly, during the desorption of adsorbed CO_2 under humid air (5% RH, 30 °C) in step III, we observe a pronounced overshoot in the TGA profiles for all three K^+-exchanged zeolites (insets in Fig. 1). We previously ascribed such an overshoot to be a manifestation of H_2O desorption during humid CO_2 adsorption in step II (*i.e.* the overshoot is a consequence of the kinetically slower water readsorption compared to CO_2 desorption in step III). When we compare TGA data of three zeolites between sequential *versus* simultaneous adsorption of H_2O and humid CO_2, the results show a path independence in humid CO_2 adsorption, demonstrating thermodynamic control (see Fig. S3, ESI†).

We characterized humid CO_2 adsorption in K^+ exchanged RHO, MER and PAU zeolites with *in situ* DRIFTS. Fig. 2 shows DRIFT spectra of each zeolite after H_2O saturation in air (step I; H_2O, spectra in black), and subsequent humid CO_2 adsorption (step II; humid CO_2, spectra in red) at a fixed relative humidity and temperature (5% RH, 30 °C) under equilibrium control. Focusing first on –OH stretching (ν) IR bands at 3800–3000 cm^{-1}, which characterize adsorbed H_2O, data shown in Fig. 2a–c show subtraction spectra that minimize overlap and interference from gas-phase CO_2 $\nu_1 + \nu_3$ and $2\nu_2 + \nu_3$ combination bands (see Fig. S4,

[a] *Department of Chemical and Biomolecular Engineering, University of California, Berkeley, California 94720, USA. E-mail: ieehwangho@berkeley.edu, askatz@berkeley.edu*
[b] *Mitsubishi Chemical Corporation, Science and Innovation Center, Aoba-ku, Yokohama 227-8502, Japan*

† Electronic supplementary information (ESI) available. See DOI: https://doi.org/10.1039/d4cc03267e

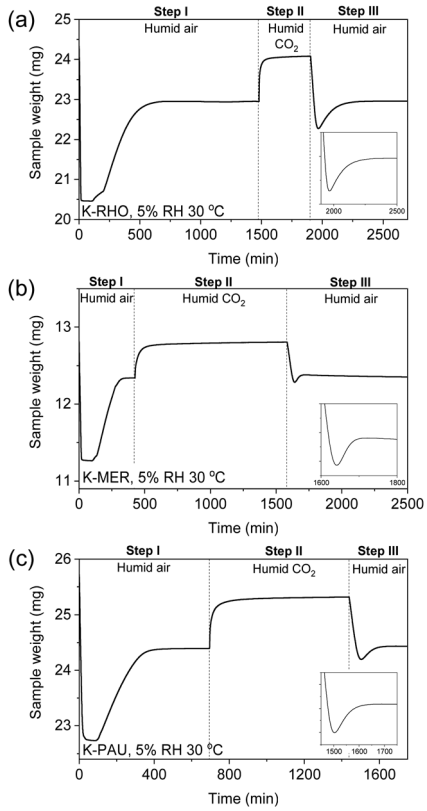

Fig. 1 TGA profiles of (a) K-RHO, (b) K-MER and (c) K-PAU zeolites during gas adsorption under humid air (step I), humid CO_2 (step II) and humid air (step III) conditions at fixed 5% RH and 30 °C.

ESI†). These DRIFTS data demonstrate a decrease in the intensity of –OH stretching bands upon humid CO_2 adsorption (step II), when compared with air at the same RH (step I). We conclude that CO_2 outcompetes H_2O in all three of these zeolites.

The insets in Fig. 2a–c show subtraction spectra that characterize the nature of the water desorbed during humid CO_2 adsorption (step II). Characteristic IR bands of such H_2O species in K-MER, K-RHO, and K-PAU are observed at 3659–3628 cm^{-1} along with a broader band at lower wavenumbers. In view of more hydrogen bonding leading to a lower wavenumber and lower extinction coefficient for –OH stretching,[14] our data demonstrate that water species with less (or the least amount of) hydrogen bonding are the ones selectively desorbed during CO_2 adsorption. We have previously assigned IR bands in this spectral region to dimeric H_2O species, which are not associated with the hydrogen bonding network of bulk water clusters in the alpha cage.[15,16] This is supported by IR band assignments in hydrated HZSM-5.[17] The subtlety of the underlying effects is demonstrated by our previous data showing no H_2O desorption upon humid CO_2 desorption in Cs-RHO, which exhibited no adsorbed dimeric water in step I, in contrast with our results here with the same zeolite exchanged with K^+ cations.[12] These results emphasize the importance of dimeric water, which we previously demonstrated adsorbs slightly more weakly than bulk H_2O in K-MER.[12]

The data above emphasize the generality of CO_2 outcompeting dimeric H_2O in zeolites possessing K^+-D8R structures, and suggest such structures as privileged structural motifs for selective CO_2 adsorption under humid conditions. To elucidate the role of K^+ cations and D8R structures in facilitating selective CO_2 adsorption in the presence of H_2O, we performed DRIFTS on the framework (T–O–T) vibration region of all three zeolites after H_2O adsorption. We observe negative IR bands at 949–962 cm^{-1} (see data in Fig. S5, ESI†). We observe further perturbation to those bands after subsequent humid CO_2 adsorption. Our prior

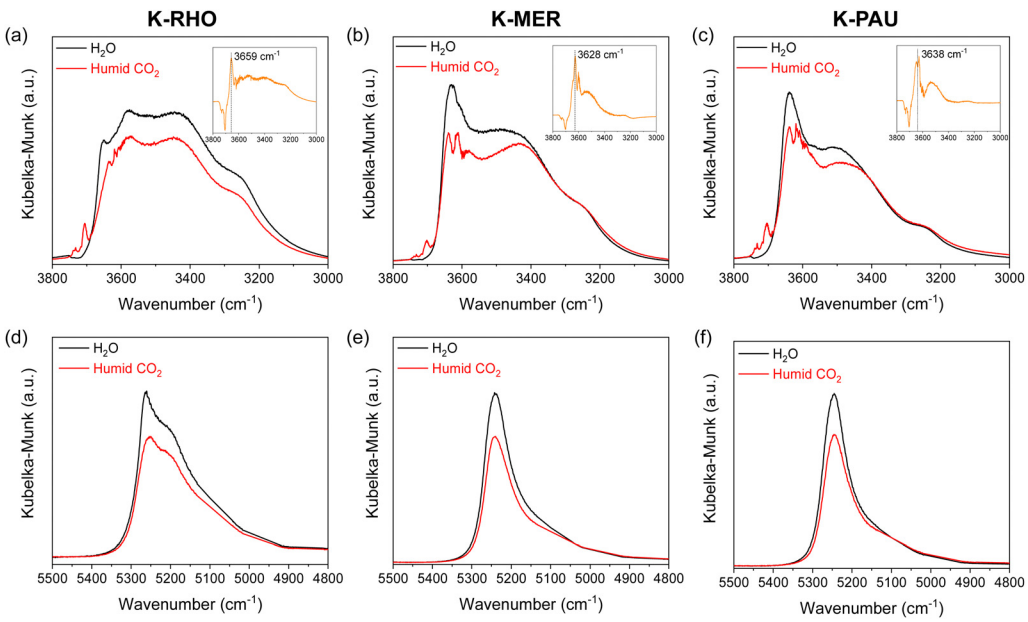

Fig. 2 (a)–(c) DRIFT spectra of the –OH stretching IR band for adsorbed H_2O in K-RHO, K-MER and K-PAU, respectively, after equilibration under humid air (H_2O, black) and subsequent humid CO_2 conditions (humid CO_2, red) at 5% RH and 30 °C. (d)–(f) DRIFT spectra of the combination IR band of H_2O in K-RHO, K-MER and K-PAU, respectively, under the same conditions.

DRIFTS study[12] proved that such IR band perturbations reflect the migration of K^+ cations from their initial position in the center of the D8R, out to the single 8-ring (S8R) site, as caused by adsorption of a H_2O dimer and/or CO_2.[18] We surmise that when CO_2 replaces dimeric H_2O dimer in the D8R in K-RHO, K-MER, and K-PAU, the further negative increases in the framework vibration (T–O–T) bands indicate that CO_2 adsorbs to the same cationic site in the D8R and pushes the cation further out away from the center. This result identifies the privileged CO_2 adsorption site as a K^+ cation located within the D8R structure of these three zeolites.

Next, we combine DRIFTS and TGA to independently quantify adsorbed water and CO_2 adsorption during step II in K^+-D8R zeolites. DRIFT spectra in Fig. 2d–f exhibit a combination IR band ($\nu + \delta$) of adsorbed H_2O in the spectral region of 5500–4800 cm^{-1}, and the integrated area of this band quantifies the amount of H_2O adsorbed in zeolite.[19] By comparing the areas of this IR band before and after humid CO_2 adsorption in steps I and II, we quantify the amount of desorbed H_2O during humid CO_2 adsorption in step II to correspond to 22%, 19%, and 16% of the total equilibrated H_2O uptake in step I (in humid air) for K-RHO, K-MER and K-PAU, respectively (Fig. 2d–f and see Fig. S6 and S7, ESI†). Combining this with TGA data in Fig. 1 and Fig. S2 (ESI†), we rigorously quantify H_2O and CO_2 uptakes in K^+-D8R zeolites, corresponding to humid CO_2 uptakes of 1.18–1.85 mmol g^{-1} (see "IR corrected" in Fig. S2, ESI†). The 1.85 mmol g^{-1} humid CO_2 uptake corresponding to K-RHO is the highest one that we have observed to date at 5% RH. This is a zeolite that does not appear to be all that impressive for humid CO_2 uptake when analysis is based on TGA data alone coupled with conventional heuristics.[8,12]

Comparing K-MER zeolites having different Si/Al ratios in our current and previous[12] study (Si/Al = 2.9 *vs.* 2.0, respectively), their humid CO_2 uptakes do not show significant difference at 5% RH and 30 °C (1.35 mmol g^{-1} *vs.* 1.27 mmol g^{-1}, respectively). This similarity was unexpected given the 3.5-fold higher dry CO_2 uptake (at 1 bar) for the K-MER zeolite at the higher Si/Al ratio (see Fig. S8, ESI†), and this speaks to the general disconnect between sites for dry and humid CO_2 adsorption in zeolites.

We quantify transient H_2O and CO_2 adsorption profiles *via* combined TGA and time-resolved DRIFTS. The profiles clearly demonstrate H_2O desorption by CO_2 adsorption in step II and reversible H_2O re-adsorption upon CO_2 desorption, under humid air, in step III (see in Fig. S9a–c, ESI†). Parametric (phase) plots in Fig. S9d–f (ESI†) demonstrate direct relationships between amounts of H_2O readsorption and CO_2 desorption during step III, ranging from 1.85 (±0.06)–2.29 (±0.13) H_2O per CO_2. We conclude that within uncertainty each molecule of CO_2 desorbed during step III is replaced with a single H_2O dimer. This macroscopic quantification connects with the qualitative microscopic observation in DRIFTS in Fig. 2 showing selective desorption of dimeric H_2O upon humid CO_2 adsorption in step II.

To better understand the role of K^+ cations, we compared H^+-exchanged forms of both RHO and PAU zeolites under humid CO_2 conditions (the structure of H-MER zeolite was unstable[20]). In stark contrast to TGA data for K^+-zeolites in Fig. 1a and b, corresponding TGA data for the H^+ form of RHO and PAU zeolites in Fig. S10a and b (ESI†) lack a characteristic overshoot in the gravimetric profiles at step III, which was present for K-RHO and K-PAU zeolites. This observation couples with the IR bands of H_2O in H-RHO and H-PAU zeolites not appreciably changing before and after humid CO_2 adsorption (*i.e.* between steps I and II; see Fig. S11, ESI†). We conclude that humid CO_2 adsorption during step II does not result in desorption of H_2O from step I in the H^+-exchanged forms of the zeolites. This underscores the important role of K^+-D8R structures as H_2O resilient sites for humid CO_2 adsorption in zeolites.

DRIFTS data in Fig. 3 demonstrate asymmetric stretching (ν_3) IR bands of adsorbed CO_2 in zeolites, which are acquired during a desorption cycle in humid air during step III. These IR bands are observed at 2353 cm^{-1}, 2346 cm^{-1}, and 2347 cm^{-1} for K-RHO, K-MER and K-PAU, respectively. In comparison, the same IR bands for H-RHO and H-PAU are located at a much lower frequency of 2342 and 2341 cm^{-1}, respectively. These observed frequency shifts between the K^+- and H^+-exchanged forms of the zeolite can be rationalized on the basis of the Stark effect.[21] This effect has been previously invoked to elucidate blue shifts in the IR stretching bands of adsorbed CO and CO_2 in zeolites, with the extent of blue shift shown to increase with exchange-cation charge density.[21,22] We conclude that the magnitude of the blue shifts observed above by DRIFTS are evidence of strong ion–dipole interactions involving CO_2 and K^+-D8R sites. The same reasoning predicts a lower vibrational frequency (weakening of C–O bond) in the absence of alkali cations, which is controlled solely by the negative charge of the zeolite framework,[23] resulting in CO_2 vibrational frequencies in the H^+-exchanged zeolites above, which are significantly lower than that of gas phase CO_2 (2349 cm^{-1}). We also observe a lower vibrational frequency for humid *versus* dry conditions as a result of water competitive adsorption in all three zeolites (see Fig. S12, ESI†).

From the perspective of H_2O, both the K^+- and H^+-exchanged forms of the zeolite have nearly the same water uptakes (see Fig. S2 and S10, ESI†). However, a significant difference is that the DRIFT spectra of the –OH stretching IR bands of adsorbed

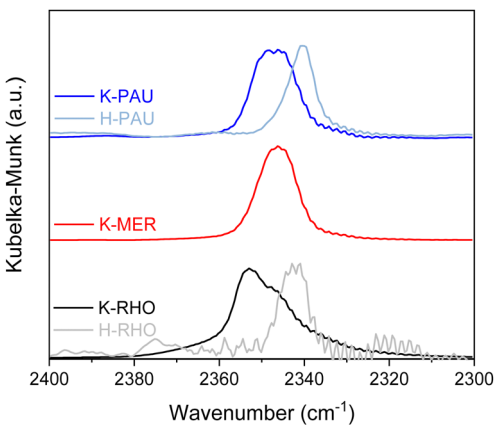

Fig. 3 DRIFT spectra of adsorbed CO_2 in K^+-D8R zeolite (K-RHO, K-MER and K-PAU) and H^+-D8R zeolites (H-RHO and H-PAU). The spectra were obtained during CO_2 desorption under humid air conditions at 5% RH and 30 °C after humid CO_2 adsorption at the same conditions.

H_2O show exclusively hydrogen-bonded water and, in particular, no dimeric H_2O for the H^+-exchanged zeolites (see Fig. 1a–c and Fig. S11, ESI†). We conclude that K^+-exchange cations in the D8R structures facilitate the synthesis of dimeric H_2O. We surmise that this is the result of two effects: (i) K^+ cations in the S8R site isolate the H_2O dimer inside of the D8R from bulk H_2O clusters on the outside, in the alpha cage, by acting as a physical barrier, and (ii) H^+ in the D8R acts as a conduit that facilitates extended hydrogen bonding between H_2O in the D8R and alpha cage, without the opportunity to site isolate a less hydrogen bonded dimeric H_2O species. Similar hydrogen-bonded conduits linking H_2O in H^+-exchanged zeolites have been previously described.[24] A consequence of K^+-D8R structures that lead to the synthesis of dimeric water in step I, which desorbs upon humid CO_2 adsorption in step II, is a higher humid CO_2 uptake compared to the corresponding H^+-exchanged zeolites (see Fig. S2 and S10, ESI†).

To further understand the importance of D8R zeolite confinement, we also investigated humid CO_2 adsorption in K-FER zeolite (Si/Al = 8.8), which consists of S8R sites that open up to a ten-membered ring (10MR) in the alpha cage. K-FER lacks the confinement afforded by K^+-D8R sites described above as those that are active for humid CO_2 adsorption.[25] While we observe a weakly hydrogen-bonded H_2O species at 3650 cm^{-1} in K-FER, which is in the range of dimeric H_2O in K^+-D8R zeolites above, both TGA and DRIFTS results of K-FER zeolite do not show evidence of H_2O being desorbed during humid CO_2 adsorption (*i.e.* neither a characteristic overshoot in TGA nor a decrease in IR band intensity of H_2O is observed; see Fig. S13, ESI†).

To understand why this isolated H_2O species in K-FER is not desorbed upon humid CO adsorption, we investigated the adsorbed CO_2 DRIFT spectra in Fig. S14 (ESI†), which show a red shift in the CO_2 IR band of K-FER (main IR band shown at 2345 cm^{-1}) compared with that in K-RHO under humid CO_2 conditions. This red shift reflects the greater confinement within the K^+-D8R structure compared to K-FER, consistent with greater confinement in zeolites causing a more blueshifted CO_2 vibrational frequency, as a consequence of more polarization and stronger ion–dipole interactions between cations and CO_2.[25] We conclude that the more open site in K-FER is ultimately responsible for weaker cation–CO_2 interactions, thereby causing a lack of competitiveness of CO_2 with a similar isolated dimeric H_2O species in K-FER. This rationalizes the higher humid CO_2 uptake in K-RHO (1.85 mmol g^{-1}) compared with K-FER (1.05 mmol g^{-1}).

It is intriguing that CO_2 outcompetes H_2O in our three cation-rich zeolites under equilibrium control, particularly when K^+ cations are known to interact strongly with water (*i.e.* they are kosmotropic in the Hofmeister series),[8] as evidenced by their significant water uptakes at the 5% RH chosen for this study. However, our results demonstrate that the local environment destabilizes dimeric H_2O in the confined K^+-D8R site compared to the more open sites in K-FER. Our work is the first demonstration of the generality of the K^+-D8R as a privileged structure for humid CO_2 adsorption, and more broadly motivates rational molecular design strategies that exploit cation-containing D8Rs for selective humid CO_2 adsorption in zeolites.

A part of this study was supported by the ''R&D Program for Promoting Innovative Clean Energy Technologies Through International Collaboration (JPNP20005)'' of the New Energy and Industrial Technology Development Organization (NEDO), Japan. AK & HL acknowledge CeRCaS NSF IUCRC funding for zeolite characterization with thermogravimetric analysis, and DOE-BES (DE-FG02-05ER15696) funding for DRIFTS studies.

Data availability

The data supporting this article have been included as part of the ESI.†

Conflicts of interest

There are no conflicts to declare.

Notes and references

1 R. S. Haszeldine, *Science*, 2009, **325**, 1647–1652.
2 M. Bui, C. S. Adjiman, A. Bardow, E. J. Anthony, A. Boston, S. Brown, P. S. Fennell, S. Fuss, A. Galindo and L. A. Hackett, *Energy Environ. Sci.*, 2018, **11**, 1062–1176.
3 D. G. Boer, J. Langerak and P. P. Pescarmona, *ACS Appl. Energy Mater.*, 2023, **6**, 2634–2656.
4 D. Fu and M. E. Davis, *Chem. Soc. Rev.*, 2022, **51**, 9340–9370.
5 J. M. Kolle, M. Fayaz and A. Sayari, *Chem. Rev.*, 2021, **121**, 7280–7345.
6 P. Guo, J. Shin, A. G. Greenaway, J. G. Min, J. Su, H. J. Choi, L. Liu, P. A. Cox, S. B. Hong and P. A. Wright, *Nature*, 2015, **524**, 74–78.
7 H. J. Choi, D. Jo, J. G. Min and S. B. Hong, *Angew. Chem., Int. Ed.*, 2020, **60**, 4307–4314.
8 L. Xu, A. Okrut, G. L. Tate, R. Ohnishi, K. L. Wu, D. Xie, A. Kulkarni, T. Takewaki, J. R. Monnier and A. Katz, *Langmuir*, 2021, **37**, 13903–13908.
9 J. A. Thompson and S. I. Zones, *Ind. Eng. Chem. Res.*, 2020, **59**, 18151–18159.
10 P. Eubank, *AIChE J.*, 1972, **18**, 454–456.
11 T. D. Pham, M. R. Hudson, C. M. Brown and R. F. Lobo, *ChemSusChem*, 2014, **7**, 3031–3038.
12 H. Lee, D. Xie, S. I. Zones and A. Katz, *J. Am. Chem. Soc.*, 2023, **146**, 68–72.
13 A. Bieniok and H.-B. Burgi, *Studies in Surface Science and Catalysis*, Elsevier, 1994, vol. 84, pp. 567–574.
14 M. Van Thiel, E. D. Becker and G. C. Pimentel, *J. Chem. Phys.*, 1957, **27**, 486–490.
15 J. N. Kondo, M. Iizuka, K. Domen and F. Wakabayashi, *Langmuir*, 1997, **13**, 747–750.
16 J. Paul, C. Collier, R. Saykally, J. Scherer and A. O'keefe, *J. Phys. Chem. A*, 1997, **101**, 5211–5214.
17 J. H. Hack, J. P. Dombrowski, X. Ma, Y. Chen, N. H. Lewis, W. B. Carpenter, C. Li, G. A. Voth, H. H. Kung and A. Tokmakoff, *J. Am. Chem. Soc.*, 2021, **143**, 10203–10213.
18 D. Fu, Y. Park and M. E. Davis, *Angew. Chem., Int. Ed.*, 2022, **61**, e202112916.
19 J.-P. Gallas, J.-M. Goupil, A. Vimont, J.-C. Lavalley, B. Gil, J.-P. Gilson and O. Miserque, *Langmuir*, 2009, **25**, 5825–5834.
20 V. M. Georgieva, E. L. Bruce, M. C. Verbraeken, A. R. Scott, W. J. CasteelJr, S. Brandani and P. A. Wright, *J. Am. Chem. Soc.*, 2019, **141**, 12744–12759.
21 C. Lamberti, S. Bordiga, F. Geobaldo, A. Zecchina and C. Otero Areán, *J. Chem. Phys.*, 1995, **103**, 3158–3165.
22 B. Bonelli, B. Civalleri, B. Fubini, P. Ugliengo, C. O. Areán and E. Garrone, *J. Phys. Chem. B*, 2000, **104**, 10978–10988.
23 S. Bordiga, C. Lamberti, F. Bonino, A. Travert and F. Thibault-Starzyk, *Chem. Soc. Rev.*, 2015, **44**, 7262–7341.
24 E. Grifoni, G. Piccini, J. A. Lercher, V.-A. Glezakou, R. Rousseau and M. Parrinello, *Nat. Commun.*, 2021, **12**, 2630.
25 D. Fu, Y. Park and M. E. Davis, *Proc. Natl. Acad. Sci. U. S. A.*, 2022, **119**, e2211544119.